OPEN ACCESS
PAPER

Mongolian Journal of Geography and Geoecology - MJGG

Received: 01 May 2025; Accepted: 10 June 2025; Published online: 1 September 2025
https://doi.org/10.5564/mjgg.v62i46.4080

Synergistic use of PRISMA hyperspectral and Sentinel-1B SAR data for land cover classification

***CORRESPONDING AUTHOR**
Damdinsuren Enkhjargal
enkhe2014@gmail.com

CITATION
Amarsaikhan D, Damdinsuren E, Odontuya G, Tsogzol G, Jargaldalai E, Boldbaatar N, Ochirhuyag L (2025). Synergistic Use of PRISMA Hyperspectral and Sentinel-1B SAR Data for Land Cover Classification. *Mongolian Journal of Geograhy and Geoecology,* 62(46), 1–7.
https://doi.org/10.5564/mjgg.v62i46.4080

Amarsaikhan Damdinsuren[1], Damdinsuren Enkhjargal[1,*], Odontuya Gendaram[2], Tsogzol Gurjav[1], Jargaldalai Enkhtuya[1], Boldbaatar Natsagdorj[1], Ochirhuyag Lkhamjav[1]

[1]*Institute of Geography and Geoecology, Mongolian Academy of Sciences,Ulaanbaatar 15170, Mongolia*
[2]*Mongolian University of Pharmaceutical Sciences, Ulaanbaatar, Mongolia*

ABSTRACT
The aim of this study is to compare the performance of deep learning, machine learning, and advanced hyperspectral image classification methods for distinguishing land cover types in Ulaanbaatar city. The study area includes various land cover classes such as built-up areas, ger districts, forests, willows, grasslands, soil, and water, with significant statistical overlaps between the built-up areas and the ger districts. For data sources, we selected PRISMA (Hyperspectral Precursor of the Application Mission) and Sentinel-1B dual-polarization synthetic aperture radar (SAR) images. Three different band combinations were utilized to identify the mixed urban land cover classes in Mongolia's capital city. To differentiate the existing classes, we employed an artificial neural network (ANN), support vector machine (SVM), and spectral angle mapper (SAM), assessing their performance against one another. To evaluate the accuracy of the classification results, we applied the Kappa coefficient. For all three band combinations, the SVM method demonstrated superior performance, with Kappa coefficients ranging from 0.96 to 0.98. The ANN showed the second-highest performance, with Kappa coefficients ranging from 0.83 to 0.96. In contrast, the SAM yielded the lowest performance, with Kappa coefficients between 0.67 and 0.71. Our study observed that the performance of the selected classification techniques depended on the chosen parameters and the structure of the datasets. Overall, this study highlights that the combined use of hyperspectral and microwave datasets can enhance the classification of land cover types, with the SVM approach emerging as the most reliable method for producing an accurate land cover map.

KEYWORDS
Deep learning, Machine learning, Hyperspectral, SAR, Image classification stock

1. INTRODUCTION

Hyperspectral image processing and analysis unfold a realm of remarkable opportunities to deepen our understanding of an object's spectral information across an expansive range of wavelengths. This technology captures an extraordinary level of detail and precision, revealing subtle variations that might otherwise go unnoticed. The examination and interpretation of land cover within these vibrant hyperspectral images play a pivotal role in illuminating the intricate workings of our planet's diverse ecosystems. By harnessing this data, we can uncover invaluable insights into the complex interplay of natural and anthropogenic factors, including the rapid encroachment of urbanization, the dynamic shifts caused by environmental changes, and the evolving landscape of agricultural practices [1-2].

Different classification techniques for hyperspectral data have been effectively applied to categorize image pixels into distinct classes [3]. Although the classification process is challenging due to the vast quantity of data samples and often limited labels, it also opens opportunities for improvement. By thoughtfully selecting the relevant bands from the image, we can significantly enhance classification outcomes and obtain more reliable predicted values, leading to better-informed decision-making in environmental planning and management [4-5].

The accurate classification of hyperspectral images is crucial, given the intricate and diverse information captured across the numerous spectral bands present in the data. Each band holds unique insights that, when correctly interpreted, can reveal significant pattems and changes within environmental systems. Achieving high classification accuracy is vital for deriving meaningful insights, which are indispensable for effectively monitoring land cover transformations and managing a variety of natural resources. Such insights not only enhance our understanding of environmental dynamics but also support sustainable practices and informed decision-making in resource management [6-7].

In recent years, a wide array of advanced algorithms, including various machine learning and deep learning techniques, have been utilized for hyperspectral image classification tasks, resulting in remarkable outcomes [8]. The application of these sophisticated methods has significantly improved the efficiency of hyperspectral image analysis and enables us to classify different land cover types with exceptional precision [9]. As a result, we can create detailed maps and forecasts that provide invaluable insights into the current condition and health of our planet's environment. This information is essential for researchers and policymakers, empowering them to make informed decisions regarding sustainable land management and conservation efforts [10].

Over the years, a wide array of sophisticated algorithms has been developed, each designed to tackle specific challenges in hyperspectral data classification [10]. However, the effectiveness of these techniques can vary significantly, largely influenced by the unique structure and inherent characteristics of the data at hand [11]. Understanding these distinctions is crucial, as they can determine how well an algorithm performs in real-world applications [11].

Therefore, in the current research, we wanted to compare the performances of deep learning, machine learning, and advanced hyperspectral image classification methods for the discrimination of land cover types in Ulaanbaatar, the capital city of Mongolia.

2. STUDY AREA, DATA SOURCES, AND PREPROCESSING

As a test area Ulaanbaatar, the capital city of Mongolia, has been selected. While the city spans 35 kilometers from west to east and 25 kilometers from north to south, this research will concentrate on a small section of the central area. The selected part extends over 4km from west to east and about 5 km from north to south. Within this area, various types of land cover are present, including built-up area, ger area, forest, willow trees, grass, soil, and water bodies.

In the present study, the selected data sets consisted of PRISMA hyperspectral images acquired on 15 August 2022, Sentinel-1B dual polarization SAR images received on 22 August 2022 and some other ground truth information. PRISMA is a medium-resolution hyperspectral imaging satellite developed and operated by the Italian Space Agency. It carries two sensor instruments, the Hyperspectral Camera (HYC) module and the Panchromatic Camera (PAN) module. The HYC module has a spatial resolution of 30 m and operates in two bands, a 66-channel visible (VIS)/near infrared (NIR) band with a spectral interval of 400-1010 nm, and a 173 channel NIR/short-wave infrared (SWIR) band with a spectral interval of 920-2505 nm. The second sensor module, PAN, is a high-resolution optical imager with one channel [12]. The SAR data was presented in IW (Interferometric Wide) GRD (Ground Range Detected) format and had a pixel resolution of 10 m.

Before the analysis, we conducted radiometric (haze correction) and geometric (2nd order transformation using 10 ground control points) corrections on the selected RS images. During this process, we discovered that the water absorption bands and several other bands from the PRISMA image contained zero values. Consequently, we excluded these bands, which reduced the original dataset from 234 bands to 202 bands. We then geometrically corrected the Hyperion bands to a UTM map projection using a topographic map of the study area at a scale of 1:100,000. Ten ground control points were selected in well-defined areas and other clear sites. For the transformation, we employed a second-order transformation method along with nearest neighbor resampling, achieving a root mean square error (RMSE) of 0.89 pixels. For the Sentinel-1B SAR images, we applied frost filtering to mitigate speckle noise before georeferencing the microwave bands to the UTM map projection, using the corrected hyperspectral image as a reference. In this instance, we implemented a linear transformation and bilinear resampling technique, resulting in an RMSE of 0.76 pixels.

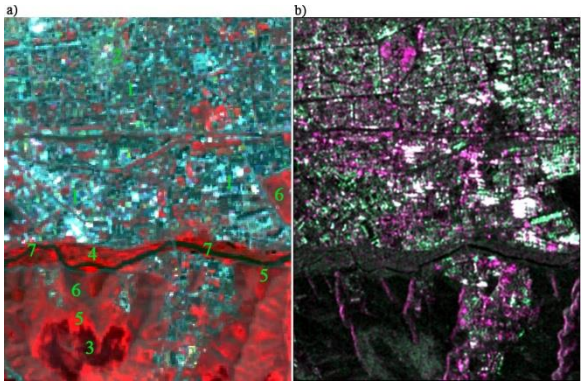

Figure 1. Test area: (a) False color image of PRISMA data (1-builtup area, 2-ger area, 3-forest, 4-willow, 5-grass, 6-soil, and 7-water), (b) Color image of Sentinel-1B (R=VV, G=VH, B=(VV+VH)/2).

Radiometrically and geometrically corrected false color image of PRISMA containing some examples of available land cover classes, and color image of Sentinel-1B of the target area are shown in Figure 1a-b.

3. RESEARCH METHODS

In this study, we used and compared such classification techniques as an ANN, SVM, and SAM for the discrimination of urban land cover classes in the selected test area.

The ANN serves as a powerful algorithm modeled after the functions of the human brain. It comes in various forms, and for this study, we have chosen to utilize the feed-forward neural network classification method. This technique is widely recognized for its effectiveness in digital data analysis [11]. In this method, neurons are systematically arranged in layers and interconnected to facilitate the seamless flow of information from the input units, through the hidden layers, to the output layer. The input units play a crucial role by transmitting signals to the hidden units in the subsequent layer. To enhance the network's ability to represent meaningful functions, it is essential to adjust the weights effectively [13]. This iterative adjustment process aims to minimize overall error, which is commonly quantified as the sum of squared errors for all input-output pairs relative to the network weights. This is accomplished through non-linear optimization methods, which further refine the network's performance [14].

The SVM is a robust and sophisticated non-parametric, supervised machine learning model that plays a pivotal role in addressing a variety of regression and classification challenges across diverse processes [15]. Its exceptional capacity for achieving high accuracy underscores the remarkable effectiveness of SVM in tackling complex high-dimensional predictions. This powerful algorithm adeptly classifies data by transforming the original data space into an enriched multidimensional feature space, where it meticulously constructs an optimal hyperplane. This hyperplane serves as a critical boundary that distinctly separates data points into classes, all while striving to maximize the margin between the nearest points of these differing classes [11]. Furthermore, when confronted with data points that resist linear separation in their original input space, SVM skillfully implements nonlinear transformations, elevating the data into a higher-dimensional realm. This elevated perspective not only enhances the algorithm's ability to identify patterns but also significantly boosts its analytical power [16].

The SAM is an advanced technique for spectral classification that adeptly matches the spectral signatures of individual pixels to established reference spectra by utilizing an n-D angle. This method is grounded in a crucial assumption: each pixel in RS imagery uniquely represents a specific type of ground cover material, allowing it to be classified into only one distinct ground cover class [17]. The SAM algorithm operates by assessing the spectral similarity between two spectra, calculating the angle that exists between them. In this context, each spectrum is envisioned as a vector existing within an n-

dimensional space, where the dimensions correspond to the number of spectral bands being analyzed. In practice, SAM evaluates the angular relationship between the vector of an endmember spectrum and the vector of each individual pixel within the n-D space. Smaller angles indicate a closer match to the reference spectrum, suggesting a higher likelihood that the pixel belongs to that specific ground cover class. Conversely, pixels that fall beyond a specified maximum angle threshold—expressed in radians—are excluded from classification, thereby enhancing the precision of the results [18].

4. RESULT AND DISCUSSION

In the study area, we observed a significant statistical overlap between the built-up area and the ger district, highlighting the complex interplay between urban land uses. Additionally, there were notable overlaps among the green classes, indicating a diverse landscape interspersed with vegetation. Therefore, in the present study, for the identification of the existing land cover classes, we tested the following band combinations:

1. The less correlated original 5 spectral bands (i.e. B2, B3, B8a, and B11) of the PRISMA data
2. All original spectral bands of the PRISMA data
3. All original spectral bands of the PRISMA data, and VV, VH, (HH+VH)/2 of Sentinel-1 data.

To effectively select training signatures from the combined images, we began by meticulously defining three to five regions of interest (ROIs) that accurately represent the distinct land cover classes through rigorous analysis. The separability of these training signatures was initially assessed in feature space, allowing us to visualize the distribution of the data. This was further evaluated using the transformed-divergence separability measure (ENVI), ensuring that the training signatures could be reliably differentiated for subsequent analysis.

After the investigation, the samples that demonstrated the greatest separability were chosen to form the final signatures. The final signatures included 987 pixels for built-up area, 471 pixels for ger area, 398 pixels for forest, 285 pixels for grass, 279 pixels for willow, 305 pixels for soil, and 205 pixels for water, respectively.

For the accuracy assessment in our study, Kappa coefficient has been used. The KC is a measure of the overall statistical agreement of an error matrix. It measures the degree of agreement between a pair of variables, frequently used as a metric of interrater reliability [19]. To ensure accurate ground truth information for the test area, we selected several regions with the purest pixels. This selection was driven by the observation that larger classes, such as built-up areas and soil, offered more available pixels for evaluation.

In the current study, we applied the SVM classifier with a radial basis function kernel, a well-regarded choice known for its effectiveness in various kernelized learning algorithms. This kernel allows the SVM to map input data into a higher-dimensional feature space, facilitating the identification of a hyperplane that effectively distinguishes between different classes [20]. For the ANN, we strategically selected a logistic activation function and incorporated two hidden layers to enhance the model's performance. Additionally, for the SAM, we determined a maximum angle of 0.25 to guide the final decision-making process, providing a clear and effective framework for our analysis.

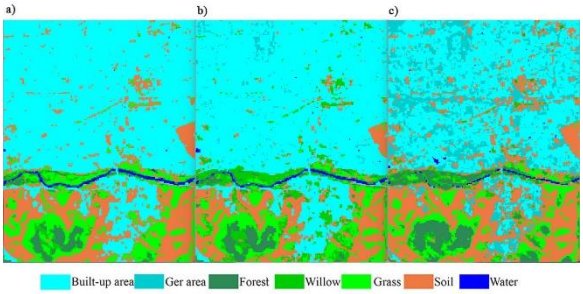

Figure 2. Comparison of classification results using 5 band combinations:
(a) the ANN, (b) the SVM, (c) the SAM.

The final classified images by the ANN, SVM, and SAM using 5 spectral bands of the PRISMA are shown in Figure 2a-c. From Figure 2a, it can be observed that the original 5 spectral bands of the hyperspectral image clearly indicate the dominance of the built-up area and soil classes. However, the ger area is not represented in the figure and is completely overshadowed by pixels belonging to the built-up area. Additionally, the willow class is mostly represented by pixels from the grass class. There are some statistical overlaps among the grass, willow, and soil classes. The ANN used for this analysis achieved a Kappa coefficient of 0.83. In contrast, the SVM method displayed the best result, as shown in Figure 2b, with a Kappa coefficient of 0.93. It is evident that the built-up area had the highest accuracy. Unlike the results from the ANN, the ger area is visible in the SVM output, which also shows clear distinctions between the willow and grass classes. As seen in Figure 2c, the SAM method yielded the lowest result, with a Kappa coefficient of 0.69. There were significant statistical

overlaps between the built-up and ger areas, as well as moderate overlaps among the other classes. It is important to note that the water class is hardly visible in the classification results and is predominantly represented by pixels from other classes. However, the soil class has more clear appearance in this classification.

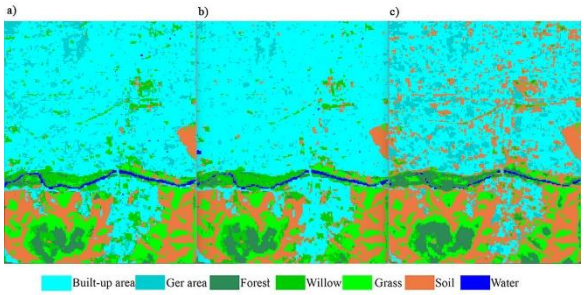

Figure 3. Comparison of classification results using 202 band combinations:
(a) the ANN, (b) the SVM, (c) the SAM.

In many instances, image processing experts believe that incorporating additional spectral bands could significantly enhance classification accuracy. To explore this potential, we proceeded to classify the original 202 bands from the PRISMA dataset. The outcomes of these classifications are depicted in Figure 3a-c. Notably, Figure 3a demonstrates that the original 202 spectral bands result in improved classification accuracy compared to the five-band combination. The ANN used in this analysis achieved a commendable Kappa coefficient of 0.95, indicating a reliable result. While there are some statistical overlaps between the built-up and ger areas, the ger district is distinctly identifiable in the classified image. Further analysis revealed that the SVM method performed exceptionally well, as illustrated in Figure 3b, achieving a Kappa coefficient of 0.98. This indicates a reduced statistical overlap between the built-up and ger areas, as well as between the willow and grass classes. Both the ANN and SVM classifiers yielded similar results for the forest and its surroundings, yet they exhibited differences in their statistical overlaps between the built-up and soil classes, highlighting areas for further investigation. The SAM method, while yielding the lowest Kappa coefficient of 0.67, showed an improvement over the five-band combination (Figure 3c). This suggests that even less sophisticated methods can enhance classification accuracy. There were still significant statistical overlaps between the built-up and ger areas, alongside moderate overlaps among other classes. In comparison to the other classes, the soil classification exhibited greater accuracy.

The integrated application of hyperspectral and SAR images provides an opportunity to enhance classification outcomes significantly. In this study, we classified all original bands from the PRISMA and Sentinel-1B dual polarization datasets. The results are represented in Figure 4a-c. In Figure 4a, it is clear that the combined utilization of multisource datasets has led to improved classification results compared to the 202-band combination, achieving an impressive Kappa coefficient of 0.96. Although some statistical overlaps persist between the built-up and ger areas, the reduction in overlaps among other classes indicates progress. The SVM method consistently emerged as the leading approach, as highlighted in Figure 4b, yielding a Kappa coefficient of 0.98. The improvement demonstrates not only reduced statistical overlaps between the built-up and ger areas but also between the willow and grass classes. This result closely resembles that of the 202-band combination, suggesting a possible pathway for further refinement. While the SAM method achieved the lowest result with a Kappa coefficient of 0.71, it is important to note this represents an improvement over the previous combinations (Figure 4c). Some significant statistical overlaps still remain between the built-up and ger areas, with moderate overlaps noted among other classes, indicating areas for future enhancement. Ultimately, it is evident that the ger district exhibits a clearer distinction compared to earlier band combinations.

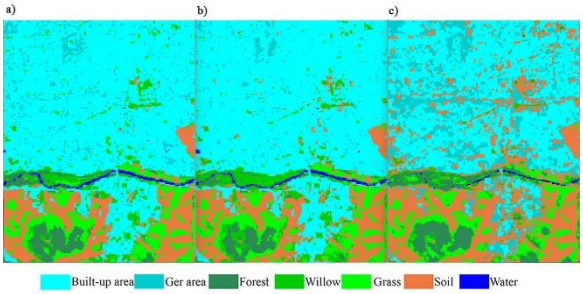

Figure 4. Comparison of classification results using 204 band combinations:
(a) the ANN, (b) the SVM, (c) the SAM.

5. CONCLUSION

The main objective of this research was to compare the performances of deep learning, machine learning, and advanced hyperspectral image classification methods in distinguishing land cover classes within Ulaanbaatar city, utilizing multisource datasets. The data sources comprised 202 bands of PRISMA hyperspectral images and Sentinel-1B dual-polarization SAR datasets. To identify the available land cover classes, three different band combinations

and three classifiers, namely, ANN, SVM, and SAM were employed. In the initial five-band combination, the SVM technique outperformed the others, achieving a Kappa coefficient of 0.93. The ANN classifier followed with a Kappa coefficient of 0.83, while the SAM technique recorded the lowest performance. In the 202-band combination, the SVM method again produced the best outcome, with a Kappa coefficient of 0.98. The ANN classifier showcased the second-best performance, achieving a Kappa coefficient of 0.95, while the SAM method once more yielded the least favorable result. Notably, the performance of the ANN improved substantially compared to the previous combination. In the 204-band combination, the SVM method maintained its lead as the top performer, with a Kappa coefficient of 0.98. The ANN classifier continued to demonstrate strong performance, achieving a Kappa coefficient of 0.96, while the SAM technique again produced the weakest result. Overall, the classification results indicated that the SVM method consistently outperformed the other techniques, while the SAM method consistently delivered the least favorable outcomes. This indicated that achieving high accuracy is not always essential for effective hyperspectral image classification methods. Instead, performance often depends on the selection of parameters, the structure of the data, and the radiometric properties of the classes. Furthermore, this study could be expanded to other relevant regions in Mongolia; however, the land cover classes may change based on the specific test area. Nonetheless, hyperspectral and SAR data from the same sources, along with the applied techniques, could still be utilized.

ACKNOWLEDGEMENTS

The authors would like to thank the Italian Space Agency for providing relevent hyperspectral data for the current study.

REFERENCES

[1] D. Amarsaikhan, A. Enkhmanlai, V. Battsengel, and V. Batsaikhan, "Feature extraction and classification of hyperspectral images", CD-ROM Proceedings of the Asian Conference on Remote Sensing (RS), Pattaya, Thailand, 2012.

[2] A. Munkh-Erdene, D. Amarsaikhan, D. Enkhjargal, G. Odontuya, and E. Jargaldalai, “Feature Extraction Approach in Hyperspectral Data BT - Proceedings of the Environmental Science and Technology International Conference (ESTIC 2021),” *Atlantis Press,* 2021, pp. 102–108, Available: doi: 10.2991/aer.k.211029.019.

[3] G. Tejasree and L. Agilandeeswari, “An extensive review of hyperspectral image classification and prediction: techniques and challenges,” *Multimed. Tools Appl*., vol. 83, no. 34, pp. 80941–81038, 2024, Available: doi: 10.1007/s11042-024-18562-9.

[4] M. Ahmad, A. M. Khan, M. Mazzara, S. Distefano, M. Ali and M. S. Sarfraz, "A Fast and Compact 3-D CNN for Hyperspectral Image Classification," *IEEE Geoscience and Remote Sensing Letters*, vol. 19, pp. 1-5, 2022, Art no. 5502205, Available: doi: 10.1109/LGRS.2020.3043710.

[5] A. Patel, D. Vyas, N. Chaudhari, R. Patel, K. Patel, and D. Mehta, “Novel approach for the LULC change detection using GIS & Google Earth Engine through spatiotemporal analysis to evaluate the urbanization growth of Ahmedabad city,” *Results Eng.,* vol. 21, p. 101788, Mar. 2024, Available: doi: 10.1016/j.rineng.2024.101788.

[6] D. Enkhjargal, D. Amarsaikhan, V. Battsengel, J. Sod-Erdene, and G. Tsogzol, "Applications of multitemporal optical images for forest resources study in Mongolia", Full paper published in CD-ROM Proceedings of the Asian Conference on RS, Nay Pyi Taw, Myanmar, 2014.

[7] J.Xie, J. Hua, S. Chen, P. Wu, P. Gao, D. Sun, Z. Lyu, S. Lyu, X. Xue, J. Lu, "HyperSFormer: A Transformer-Based End-to-End Hyperspectral Image Classification Method for Crop Classification", *Remote Sens*. 2023, 15, 3491, Available: doi:10.3390/rs15143491.

[8] M. F. Guerri, C. Distante, P. Spagnolo, F. Bougourzi, and A. Taleb-Ahmed, “Deep learning techniques for hyperspectral image analysis in agriculture: A review,” ISPRS Open J. Photogramm. *Remote Sens.,* vol. 12, no. March, p. 100062, 2024, Available: doi: 10.1016/j.ophoto.2024.100062.

[9] Q. Shenming, L. Xiang, and G. Zhihua, “A new hyperspectral image classification method based on spatial-spectral features,” *Sci. Rep*., vol. 12, no. 1, pp. 1–16, 2022, Available: doi: 10.1038/s41598-022-05422-5.

[10] D. Amarsaikhan, A. Enkhmanlai, Ts. Bat-Erdene, E. Jargaldalai, and Ch. Bolorchuluun, "Feature extraction and classification of hyperspectral data of Mongolia using machine learning methods", Full paper published in eProceedings of the Asian Conference on RS, Ulaanbaatar, Mongolia, 2022.

[11] E. Amarsaikhan, D. Enkhjargal, E. Jargaldalai, and D. Amarsaikhan, "Comparison of machine learning and parametric methods for the discrimination of urban land cover types," *Geocarto Int.*, vol. 39, Jan. 2024, Available: doi: 10.1080/10106049.2024.2380372.

[12] PRISMA (Hyperspectral), [Online]. Available: www.eoportal.org/satellite-missions/ prisma-hyperspectral, 2023.

[13] A. Malekian and N. Chitsaz, "Chapter 4 - Concepts, procedures, and applications of artificial neural network models in streamflow forecasting", Editor(s): Priyanka Sharma, Deepesh Machiwal, Advances in Streamflow Forecasting, *Elsevier*, Pages 115-147, 2021, Available: doi:10.1016/B978-0-12-820673-7.00003-2.

[14] V. F. Rodriguez-Galiano and M. Chica-Rivas, "Evaluation of different machine learning methods for land cover mapping of a Mediterranean area using multi-seasonal Landsat images and Digital Terrain Models," *Int. J. Digit. Earth,* vol. 7, no. 6, pp. 492–509, 2014, Available: doi: 10.1080/17538947.2012.748848.

[15] V. Sharma et al., "Insights into the recent advances of agro-industrial waste valorization for sustainable biogas production," *Elsevier*, vol. Volume 390, p. 129829, 2023, Available: doi:10.1016/j.biortech.2023.129829.

[16] Y. Zhang, X. Sun, S. G. Bajwa, S. Sivarajan, J. Nowatzki, and M. Khan, "Chapter Nine - Plant Disease Monitoring With Vibrational Spectroscopy," *Elsevier,* vol. 80, pp. 227–251, 2018, Available: doi: 10.1016/bs.coac.2018.03.006.

[17] S. Rashmi, S. Addamani, Venkat, and S. Ravikiran, "Spectal Angle Mapper Algorithm for remote Sensing Image Classification," *Int. J. Innov. Sci. Eng. Technol*., vol. 1, no. 4, pp. 201–205, 2014.

[18] Spectral Angle Mapper, [Online]. Available: //step.esa.int/main/wp-content/help/ versions/9.0.0/snap-toolboxes/org.esa.s2tbx.s2tbx.spectral.angle.mapper.ui/sam/SAMProcessor.html

[19] E. Nyamjargal, A. Enkhmanlai, D. Amarsaikhan, and S. Enkhtuya, "Evaluation of principal components for land cover discrimination using object-based classification", Full paper published in eProceedings of the Asian Conference on RS, Ulaanbaatar, Mongolia, 2022.

[20] Y. W. Chang, C. J. Hsieh, K. W. Chang, M. Ringgaard, and C. J. Lin, "Training and testing low-degree polynomial data mappings via linear SVM," *J. Mach. Learn. Res*., vol. 11, no. April, pp. 1471–1490, 2010.